Experimental Demonstration of Quantum Steering Swapping with Gaussian Entangled States

Na Wang, Meihong Wang,* Caixing Tian, Xiaowei Deng, and Xiaolong Su*

As a key element in quantum repeaters, entanglement swapping establishes entanglement between two independent entangled states. Besides entanglement, quantum steering has been identified as an essential quantum resource and has broad applications in quantum communication. Although entanglement swapping has been realized experimentally, quantum steering swapping still remains a challenge since the condition of quantum steering is stronger than that of entanglement. In this article, quantum steering swapping between a three-mode and a two-mode Gaussian entangled state in a lossy channel is demonstrated. By choosing the optimum gain in the classical channel that corresponds to the maximum transmission distance, the one-way and two-way steerabilities in a new three-mode Gaussian state located in distant nodes are achieved. The obtained collective steerability from two users to one user has potential application in quantum secret sharing. The results make a crucial step toward applications of quantum steering in asymmetric quantum information processing.

1. Introduction

Toward building a quantum internet, it is essential to achieve long-distance quantum communication among space-separated quantum nodes. For quantum communication with entangled states, it is a key challenge to identify suitable methods to share entangled states between users. Entanglement swapping provides a feasible method to connect space-separated quantum nodes, which establishes entanglement between space-separated independent entangled states without direct interaction.[1–4] Since one mode of an entangled state is teleported in entanglement swapping, it is also known as quantum teleportation of

entangled states.[2–4] Experimental demonstration of entanglement swapping has been achieved in the discrete-variable (DV),[5,6] continuous-variable (CV),[7–9] and hybrid CV-DV[10,11] systems. Recently, the all-optical quantum entanglement swapping has also been demonstrated.[12]

Entanglement, Einstein–Podolsky–Rosen (EPR) steering, and Bell nonlocality are all important quantum resources in quantum communication and quantum networks.[13–16] In the verification of entanglement, trusted measurement devices are used, while untrusted measurement devices are used in the verification of Bell nonlocality.[17] Different from entanglement and Bell nonlocality, EPR steering is verified in a semi-device independent way, which has no assumption

of full trust for measurement equipment on one side.[17–22] Because of the inherent asymmetry of quantum steering,[23,24] one-way EPR steering is observed,[25] which has potential applications in the tasks of quantum communication, for instance, one-sided device-independent (1sDI) quantum key distribution,[26–28] sub-channel discrimination,[29,30] quantum teleportation,[31,32] and quantum secret sharing (QSS).[33,34] EPR steering has been demonstrated in the optical system,[25,34–46] atomic system,[47,48] and high-dimensional system.[49–52] Recently, the distillation[53,54] and sudden death[55] of EPR steering have also been experimentally demonstrated.

To build a quantum network with quantum steering, it is essential to share steerability among users. Toward long-distance quantum communication with quantum steering, how to establish steerability among space-separated quantum nodes without direct interaction remains a challenging problem. Quantum steering swapping, which is also known as quantum teleportation of quantum steering, provides a feasible solution for this problem,[56,57] while it remains a challenge in experiment. Different from entanglement swapping, different types of steerabilities can be obtained after the quantum steering swapping and they can be optimized by choosing different gains.[56,57] It is impossible to optimize all types of steerabilities with an optimum gain factor. Thus, how to choose the gain factor in the classical channel according to the requirement of application of steerability is an important issue in quantum steering swapping.

In this letter, we experimentally demonstrate quantum steering swapping between a three-mode and a two-mode Gaussian entangled state in a lossy channel. By performing a joint

N. Wang, M. Wang, C. Tian, X. Deng, X. Su
State Key Laboratory of Quantum Optics and Quantum Optics Devices
Institute of Opto-Electronics
Shanxi University
Taiyuan 030006, China
E-mail: wangmh@sxu.edu.cn; suxl@sxu.edu.cn
N. Wang, M. Wang, C. Tian, X. Su
Collaborative Innovation Center of Extreme Optics
Shanxi University
Taiyuan, Shanxi 030006, China
X. Deng
Shenzhen Institute for Quantum Science and Engineering
Southern University of Science and Technology
Shenzhen 518055, China

The ORCID identification number(s) for the author(s) of this article can be found under https://doi.org/10.1002/lpor.202300653
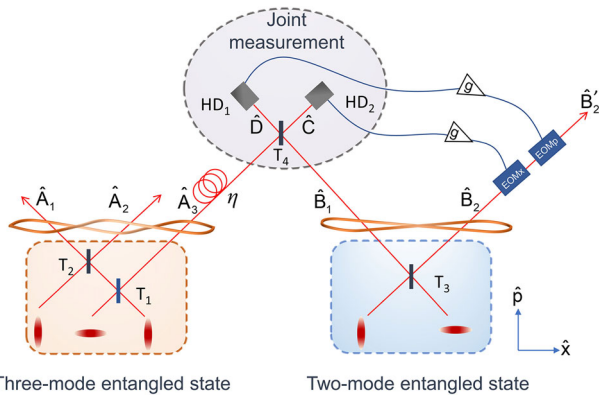
Figure 1. Schematic of the quantum steering swapping between a three-mode and a two-mode Gaussian entangled states. HD, homodyne detector; g, the gain in the classical channel; EOMx and EOMp, electro-optical amplitude and phase modulators.

measurement on two modes from two entangled states and feed-forwarding the measurement results to the other mode of the two-mode entangled state, a new three-mode Gaussian state with steerabilities is obtained. In the experiment, the optimum gain in the classical channel corresponding to the maximum transmission distance is chosen. Based on the reconstructed covariance matrices of the output three-mode state after quantum steering swapping for different transmission efficiencies, one-way and two-way steerabilities for different splittings are demonstrated. The results show that EPR steerability from one mode to another mode does not exist, only the collective steerabilities between one and the other two modes exist. The obtained collective steerability from two modes to one mode has potential application in QSS, and the one-way steerablities would be benefcial for the asymmetric quantum information processing.

2. The Principle

The principle of quantum steering swapping is shown in **Figure 1**. A three-mode CV Greenberger–Horne–Zeilinger (GHZ) state and a two-mode CV EPR state are prepared independently by coupling three and two squeezed states on beamsplitters, respectively. In the quantum steering swapping, one mode $(\hat{A}_3)$ of the three-mode CV GHZ state is transmitted through a lossy channel with transmission efficiency η. Then, the joint measurement (Bell state measurement) is performed by coupling the transmitted mode and one of the EPR states on a 1:1 beamsplitter and the output states are measured by homodyne detectors. The measurement results are fed forward to the mode $\hat{B}_2$ through classical channels to implement phase space displacement operation. Finally, the steerabilities among space-separated modes $\hat{A}_1$, $\hat{A}_2$, and $\hat{B}_2'$ are verified.

In the CV quantum information processing, the information is encoded in the amplitude and phase quadratures of photonics harmonic oscillators,[58] which are expressed by $\hat{x} = \hat{a} + \hat{a}^\dagger$ and $\hat{p} = (\hat{a} - \hat{a}^\dagger)/i$, respectively. In this case, variances of a vacuum state are $V_{\hat{x}_0} = V_{\hat{p}_0} = V_0 = 1$, where the subscript 0 represents a vacuum state. By coupling two $\hat{x}$-squeezed states and a $\hat{p}$-squeezed state on two beamsplitters with a transmittances of $T_1 = 1/3$ and $T_2 = 1/2$, a three-mode CV GHZ state consist-

ing of modes $\hat{A}_1$, $\hat{A}_2$, and $\hat{A}_3$ is obtained (see Section S1, Supporting Information, for more details). The quantum correlations between phase and amplitude quadratures of the three-mode CV GHZ state are $\Delta^2(\hat{p}_{A_1} + \hat{p}_{A_2} + \hat{p}_{A_3}) = 3V_s$ and $\Delta^2(\hat{x}_{A_1} - \hat{x}_{A_2}) = \Delta^2(\hat{x}_{A_1} - \hat{x}_{A_3}) = \Delta^2(\hat{x}_{A_2} - \hat{x}_{A_3}) = 2V_s$, respectively, where V_s is the variance of the squeezed quadrature. A two-mode CV EPR state is prepared by coupling a $\hat{p}$-squeezed state and an $\hat{x}$-squeezed state on a beamsplitter with transmittance of $T_3 = 1/2$. The quantum correlations between amplitude and phase quadratures of the two-mode state ($\hat{B}_1$ and $\hat{B}_2$) are $\Delta^2(\hat{x}_{B_1} - \hat{x}_{B_2}) = 2V_s$ and $\Delta^2(\hat{p}_{B_1} + \hat{p}_{B_2}) = 2V_s$, respectively.

The mode $\hat{A}_3$ turns into $\hat{A}_3' = \sqrt{\eta}\hat{A}_3 + \sqrt{1-\eta}\hat{v}$ after the transmission in a lossy channel, where η and $\hat{v}$ are the transmission efficiency of quantum channel and a vacuum mode introduced by loss, respectively. To implement the joint measurement, the received mode $\hat{A}_3'$ and the mode $\hat{B}_1$ are coupled on a beamsplitter with transmissivity $T_4 = 1/2$ and the amplitude quadrature $\hat{x}_C = (\hat{x}_{A_3'} - \hat{x}_{B_1})/\sqrt{2}$ and phase quadrature $\hat{p}_D = (\hat{p}_{A_3'} + \hat{p}_{B_1})/\sqrt{2}$ of output modes are measured by homodyne detectors. The measurement results are fed forward to the remaining mode $\hat{B}_2$ by two classical channels with gain g. The mode $\hat{B}_2$ is displaced by adding the feedforward signals to electro-optical amplitude and phase modulators. The displaced mode $\hat{B}_2'$ is expressed as $\hat{B}_2' = \hat{B}_2 + \sqrt{2}g\hat{x}_C + i\sqrt{2}g\hat{p}_D$.

The property of a Gaussian state with a bipartite system N and M can be determined by its covariance matrix

$$\sigma_{NM} = \begin{pmatrix} \mathcal{N} & C \\ C^{\mathsf{T}} & \mathcal{M} \end{pmatrix} \tag{1}$$

Here, matrix element $\sigma_{ij} = \langle \hat{\xi}_i \hat{\xi}_j + \hat{\xi}_j \hat{\xi}_i \rangle /2 - \langle \hat{\xi}_i \rangle \langle \hat{\xi}_j \rangle$, and $\hat{\xi} \equiv (\hat{x}_1^N, \hat{p}_1^N, \ldots, \hat{x}_n^N, \hat{p}_n^N, \hat{x}_1^M, \hat{p}_1^M, \ldots, \hat{x}_m^M, \hat{p}_m^M)^{\mathsf{T}}$ represents the vector of amplitude and phase quadratures of optical modes. The submatrices $\mathcal{N}$ and $\mathcal{M}$ are diagonal blocks of reduced states of subsystems, C and C^{T} are off-diagonal matrices of intermodal correlations between subsystems. The covariance matrix of the output three-mode state is expressed as

$$\sigma_{A_1 A_2 B_2'} = \begin{pmatrix} \sigma_{A_1} & \sigma_{A_1 A_2} & \sigma_{A_1 B_2'} \\ \sigma_{A_1 A_2}^{\mathsf{T}} & \sigma_{A_2} & \sigma_{A_2 B_2'} \\ \sigma_{A_1 B_2'}^{\mathsf{T}} & \sigma_{A_2 B_2'}^{\mathsf{T}} & \sigma_{B_2'} \end{pmatrix} \tag{2}$$

The submatrices in the Equation (2) are given by

$$\sigma_{A_1} = \sigma_{A_2} = \begin{pmatrix} \frac{1}{3}(V_a + 2V_s) & 0 \\ 0 & \frac{1}{3}(2V_a + V_s) \end{pmatrix}$$

$$\sigma_{B_2'} = \begin{pmatrix} V_{x_{B_2'}} & 0 \\ 0 & V_{p_{B_2'}} \end{pmatrix}$$

$$\sigma_{A_1 A_2} = \begin{pmatrix} \frac{1}{3}(V_a - V_s) & 0 \\ 0 & \frac{1}{3}(V_s - V_a) \end{pmatrix}$$

$$\sigma_{A_1 B_2'} = \sigma_{A_2 B_2'} = \begin{pmatrix} \frac{1}{3}\sqrt{\eta}g(V_a - V_s) & 0 \\ 0 & \frac{1}{3}\sqrt{\eta}g(V_s - V_a) \end{pmatrix} \tag{3}$$
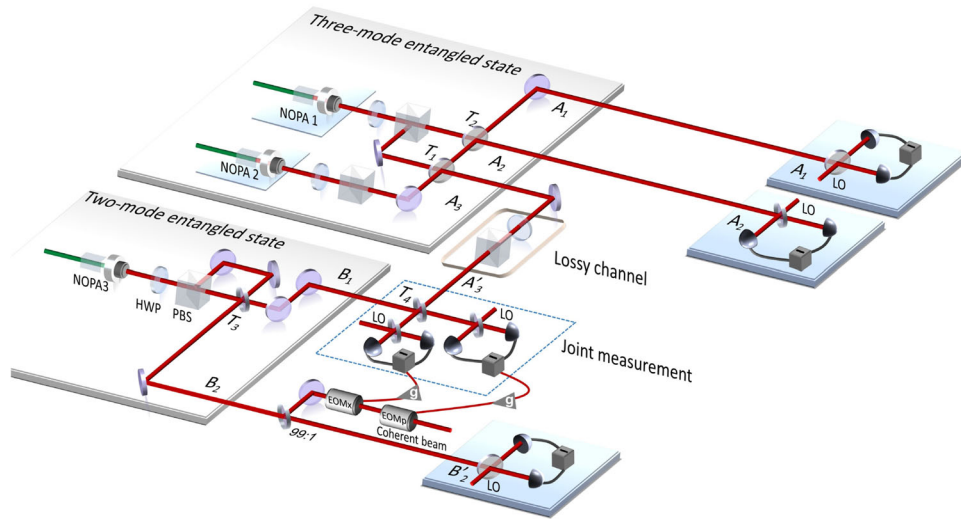
Figure 2. Experimental setup. The measurement results of the joint measurement are fed forward to a coherent beam through classical channels with gain g and electro-optical amplitude and phase modulators (EOMx and EOMp). The modulated coherent beam is coupled with mode $\hat{B}_2$ on a 99:1 beamsplitter. A half-wave plate and a polarization beamsplitter are used to simulate a lossy channel. The output states $\hat{A}_1$, $\hat{A}_2$, and $\hat{B}_2'$ after the quantum steering swapping are measured by three homodyne detectors. LO, local oscillator.

where V_a is the variance of the anti-squeezed quadrature, $V_{x_{B_2'}} = [4\eta g^2 + 3(1+g)^2]V_s/6 + [2\eta g^2 + 3(1-g)^2]V_a/6 + (1-\eta)g^2 V_0$ and $V_{p_{B_2'}} = [2\eta g^2 + 3(1+g)^2]V_s/6 + [4\eta g^2 + 3(g-1)^2]V_a/6 + (1-\eta)g^2 V_0$ are the variances of amplitude and phase quadratures of the displaced mode $\hat{B}_2'$.

Based on the covariance matrix, Gaussian steerability between two partitions ($N \to M$) can be quantified, which is given by[59]

$$\mathcal{G}^{N \to M}(\sigma_{NM}) = \max\left\{0, -\sum_{j:\bar{v}_j^{NM\backslash N}<1} \ln(\bar{v}_j^{NM\backslash N})\right\} \quad (4)$$

In the Equation (4), $\bar{v}_j^{NM\backslash N}$ ($j = 1, \ldots, m$) is the symplectic eigenvalues of the Schur complement $\bar{\sigma}_{NM\backslash N} = \mathcal{M} - C^T \mathcal{N}^{-1} C$ of subsystem N. When $\mathcal{G}^{N \to M} > 0$, the subsystem N can steer the subsystem M. The higher value of $\mathcal{G}^{N \to M}$, the stronger steerability. By swapping the roles of $\mathcal{N}$ and $\mathcal{M}$, the subsystem N can be steered by the subsystem M.

3. The Experiment and Results

The experimental setup is illustrated in **Figure 2**. The nondegenerate optical parametric amplifier (NOPA) consists of a type-II potassium titanyl phosphate (KTP) crystal and a concave mirror (see Section S2, Supporting Information, for more details). Squeezed states with −5.90 dB squeezing ($V_s = 0.26$) and 9.84 dB anti-squeezing ($V_a = 9.64$) at 1080 nm are generated from three NOPAs operated at deamplification condition, which is achieved by locking the relative phase difference between the seed and pump beams of the NOPAs to π.[60] The output coupled modes of the NOPA at +45° and −45° polarization directions (separated by a polarization beamsplitter) are $\hat{x}$-squeezed and $\hat{p}$-squeezed

states, respectively, when the half-wave plate after the NOPA is set to 22.5°. To produce the three-mode CV GHZ state, three squeezed states (generated by NOPA1 and NOPA2) are coupled on beam splitters T_1 and T_2. To produce the two-mode CV EPR state, two squeezed states generated by the third NOPA (NOPA3) are coupled on beamsplitter T_3. The mode $\hat{A}_3$ is transmitted through a lossy channel, which is simulated by a half-wave plate and a polarization beamsplitter. In order to realize joint measurement, the transmitted mode $\hat{A}_3'$ is coupled with the mode $\hat{B}_1$ on a 1:1 beamsplitter T_4, and two homodyne detectors are used to measure the amplitude and phase quadratures, respectively. The measurement results $\hat{x}_C$ and $\hat{p}_D$ are fedforward to an auxiliary coherent beam by electro-optical amplitude and phase modulators (EOMx and EOMp) first, and then the displaced auxiliary coherent beam is coupled with the mode $\hat{B}_2$ on a 99:1 beamsplitter. Thus the displaced mode $\hat{B}_2'$ is obtained.

In the quantum steering swapping, the gain g in the classical channel is an important parameter. In case of infinite squeezing, the gain in the classical channel is unit. While in the case of finite squeezing, the optimum gain can be chosen to maximize the steerability and reduce the requirement of squeezing,[56,57] which is helpful to extend the transmission distance. Here, we analyze the dependence of different types of steerabilities on gain g and transmission efficiency η at the current squeezing level, as shown in **Figure 3**, according to the covariance matrix of quantum state after the quantum steering swapping. It is obvious that different transmission distances can be achieved for different types of collective steerabilities (Figure 3a). The longest transmission distance ($\eta = 0.29$) is obtained for the steerabilities $\mathcal{G}^{A_1 \to A_2 B_2'}$ and $\mathcal{G}^{A_2 \to A_1 B_2'}$ with the optimum gain $g = 0.85$ in the classical channel. The obtainable transmission distances for the steerabilities $\mathcal{G}^{A_2 B_2' \to A_1}$, $\mathcal{G}^{A_1 B_2' \to A_2}$, $\mathcal{G}^{A_1 A_2 \to B_2'}$, and $\mathcal{G}^{B_2' \to A_1 A_2}$ are shorter than that of $\mathcal{G}^{A_1 \to A_2 B_2'}$ and $\mathcal{G}^{A_2 \to A_1 B_2'}$ when the corresponding optimum gains are chosen.

ADVANCED
SCIENCE NEWS

www.advancedsciencenews.com

LASER
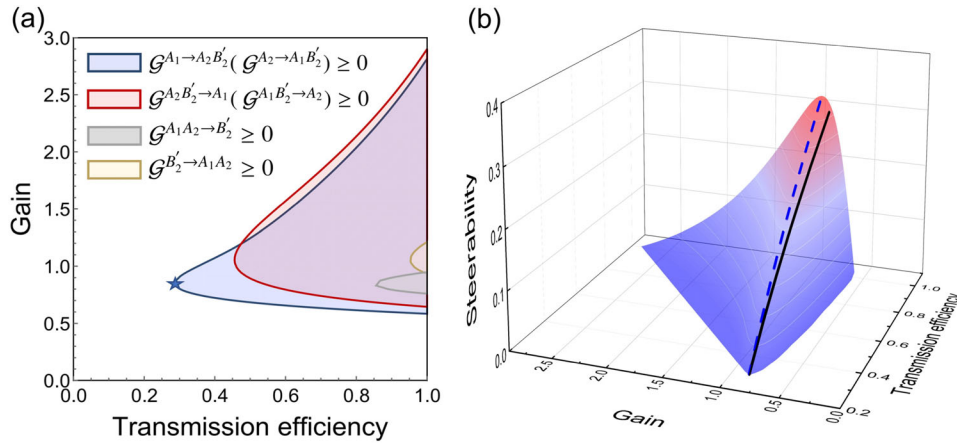& PHOTONICS
REVIEWS

www.lpr-journal.org

Figure 3. a) The dependence of different types of steerabilities on transmission efficiency and gain of classical channel. Curves represent boundaries with and without quantum steering. The blue star represents the gain in the experiment. b) The dependence of the steerability $\mathcal{G}^{A_1 \rightarrow A_2 B_2'}$ on transmission efficiency and gain. Blue dashed and black solid lines represent the maximum steerability and the steerability with $g = 0.85$, respectively.

As shown in Figure 3b, the maximum steerability $\mathcal{G}^{A_1 \rightarrow A_2 B_2'}$ is obtained with the increase of gain and transmission efficiency. The gain approaches 0.94 when $\eta = 1$ (blue dashed line in Figure 3b). To achieve the maximum steerabilities, the gain should be optimized in the range of [0.85, 0.94] for different transmission efficiencies. We choose $g = 0.85$ for different transmission efficiencies in the experiment, which simplifies the experimental difficulty and only reduce the achievable steerability slightly (black solid line in Figure 3b).

We reconstruct the covariance matrices of the output three-mode Gaussian state at transmission efficiencies $\eta = 0.98$, 0.8, 0.6, 0.4, and 0.2, respectively, which are given by

$$
\sigma_1 = \begin{pmatrix} 3.05 & 0 & 2.72 & 0.21 & 2.67 & 0.035 \\ 0 & 5.34 & -0.2 & -2.54 & -0.16 & -2.88 \\ 2.72 & -0.2 & 3.42 & 0 & 3.11 & 0.03 \\ 0.21 & -2.54 & 0 & 6.37 & 0.25 & -2.94 \\ 2.67 & -0.16 & 3.11 & 0.25 & 3.36 & 0 \\ 0.035 & -2.88 & 0.03 & -2.94 & 0 & 6.57 \end{pmatrix},
$$

$$
\sigma_2 = \begin{pmatrix} 2.68 & 0 & 2.44 & 0.11 & 2.5 & 0.11 \\ 0 & 4.75 & -0.08 & -2.42 & -0.18 & -2.51 \\ 2.44 & -0.08 & 3.51 & 0 & 3.31 & 0.13 \\ 0.11 & -2.42 & 0 & 6.44 & 0.02 & -3.08 \\ 2.5 & -0.18 & 3.31 & 0.02 & 3.67 & 0 \\ 0.11 & -2.51 & 0.13 & -3.08 & 0 & 6.53 \end{pmatrix},
$$

$$
\sigma_3 = \begin{pmatrix} 2.39 & 0 & 2.17 & 0.15 & 2.24 & 0.01 \\ 0 & 3.89 & 0.008 & -1.97 & -0.13 & -2.24 \\ 2.17 & 0.008 & 3.51 & 0 & 3.31 & 0.06 \\ 0.15 & -1.97 & 0 & 6.44 & 0.02 & -3.11 \\ 2.24 & -0.13 & 3.31 & 0.02 & 3.67 & 0 \\ 0.01 & -2.24 & 0.06 & -3.11 & 0 & 6.57 \end{pmatrix},
$$

$$
\sigma_4 = \begin{pmatrix} 1.92 & 0 & 1.72 & 0.42 & 1.8 & 0.3 \\ 0 & 2.93 & -0.03 & -1.57 & -0.07 & -1.6 \\ 1.72 & -0.03 & 3.51 & 0 & 3.31 & 0.06 \\ 0.42 & -1.57 & 0 & 6.44 & 0.02 & -3.16 \\ 1.8 & -0.07 & 3.31 & 0.02 & 3.67 & 0 \\ 0.3 & -1.6 & 0.06 & -3.16 & 0 & 6.68 \end{pmatrix},
$$

$$
\sigma_5 = \begin{pmatrix} 1.56 & 0 & 1.2 & 0.27 & 1.29 & 0.28 \\ 0 & 2.23 & -0.16 & -1.16 & -0.18 & -1.17 \\ 1.2 & -0.16 & 3.51 & 0 & 3.31 & 0.13 \\ 0.27 & -1.16 & 0 & 6.44 & 0.02 & -3.08 \\ 1.29 & -0.18 & 3.31 & 0.02 & 3.67 & 0 \\ 0.28 & -1.17 & 0.13 & -3.08 & 0 & 6.53 \end{pmatrix}. \tag{5}
$$

By substituting the reconstructed covariance matrices in Equation (5-7) into Equation (4), we obtain various types of steerabilities between any two modes and that between one and the other two modes. **Figure 4** shows the obtained steerabilities of different splittings after the quantum steering swapping in a lossy channel, which is different from the results of entanglement swapping due to the inherent asymmetric property of quantum steering. The steerabilities between any two modes do not exist, because it is limited by the monogamy relation in a three-mode state, which shows that one mode cannot be steered by two distinct modes simultaneously.[61,62] For a three-mode CV GHZ state, if the mode $\hat{B}_2'$ could be steered by the mode $\hat{A}_1$, it should be also steered by the mode $\hat{A}_2$, which is forbidden by the monogamy relation.[61,62]

Only the collective steerabilities between one and the other two modes are observed after the quantum steering swapping. For splitting $\hat{A}_1 | \hat{A}_2 \hat{B}_2'$, two-way steering $\mathcal{G}^{A_1 \rightleftharpoons A_2 B_2'}$ exists in the transmission efficiency range of $0.53 < \eta < 1$ (around 13 km in a fiber channel with loss of 0.2 dB km^{-1}). When the transmission efficiency decreases from 0.53 to 0.29, the cooperation by modes $\hat{A}_2$ and $\hat{B}_2'$ can not steer the mode $\hat{A}_1$, but only one-way steerability $\mathcal{G}^{A_1 \rightarrow A_2 B_2'} > 0$ is achieved, as shown in Figure 4a. The

ADVANCED
SCIENCE NEWS

www.advancedsciencenews.com

LASER
& PHOTONICS
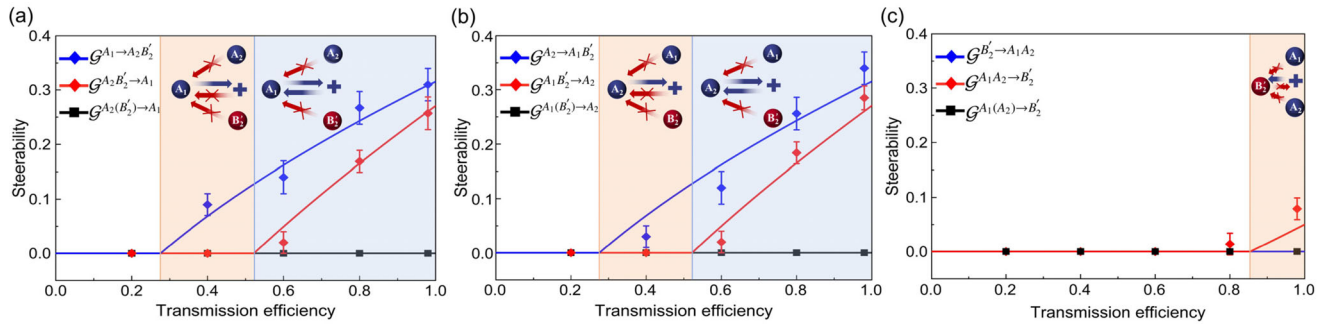REVIEWS

www.lpr-journal.org

Figure 4. Experimental results for different types of steerabilities after the quantum steering swapping in a lossy channel. a–c) The collective steerabilities for splittings $\hat{A}_1|\hat{A}_2\hat{B}'_2$, $\hat{A}_2|\hat{A}_1\hat{B}'_2$, $\hat{B}'_2|\hat{A}_1\hat{A}_2$ and the steerabilities between any two modes under Gaussian measurements. Blue and orange regions correspond to the two-way and one-way steerable regions, respectively. Error bars represent ± one standard deviation and are obtained based on the statistics of measured covariance matrices.

maximum transmission distance for the quantum steering swapping is obtained when $\eta > 0.29$ (around 26 km in a fiber channel) at present experimental parameters since the optimum gain is chosen to maximize the transmission distance for steerability of $\mathcal{G}^{A_1 \to A_2 B'_2}$ in the experiment.

The steerablities for splitting $\hat{A}_2|\hat{A}_1\hat{B}'_2$ are the same as that for $\hat{A}_1|\hat{A}_2\hat{B}'_2$, as shown in Figure 4a,b. The physical reason is that modes $\hat{A}_1$ and $\hat{A}_2$ are completely symmetric even after the quantum steering swapping. The steerabilities for splitting $\hat{B}'_2|\hat{A}_1\hat{A}_2$ are shown in Figure 4c. Only the one-way steering $\mathcal{G}^{A_1 A_2 \to B'_2} > 0$ is obtained in the transmission efficiency range of $0.85 < \eta < 1$ (around 3 km in a fiber channel). Comparing Figures 4a, 4b, and 4c, the obtained steerability of $\mathcal{G}^{A_1 A_2 \to B'_2}$ is lower than the steerabilities of $\mathcal{G}^{A_1 \to A_2 B'_2}$, $\mathcal{G}^{A_2 \to A_1 B'_2}$, $\mathcal{G}^{A_2 B'_2 \to A_1}$, and $\mathcal{G}^{A_1 B'_2 \to A_2}$, which is limited by the finite squeezing in the experiment. The dependences of experimental data on transmission efficiency agree well with the theoretical predictions, although a few data points are not exactly located on the theoretical curve (see Section S2, Supporting Information, for more details). The difference comes from the imperfections in our experimental system, including the phase fluctuation in the locking system and the stability of the whole experimental system.

4. Discussion and Conclusion

After the quantum steering swapping, the shared steerabilities among three nodes can be applied to implement quantum communication protocols. For instance, a three-mode state with the steerabilities $\mathcal{G}^{ij \to k} > 0$ and $\mathcal{G}^{i \to k} = \mathcal{G}^{j \to k} = 0$, where the modes $\hat{i}$ and $\hat{j}$ can not steer the mode $\hat{k}$ individually and only the collaboration of them presents steerability on the mode $\hat{k}$, can be applied to implement QSS.[33] In our case, QSS can be implemented with the three-mode state containing modes $\hat{A}_1$, $\hat{A}_2$, and $\hat{B}'_2$. For example, when the mode $\hat{A}_1$ or $\hat{A}_2$ acts as a dealer to send a secret and the remaining two modes act as players to decode the secret with cooperation, QSS can be implemented in the range of $0.53 < \eta < 1$.

Toward further applications of the obtained quantum steering, there are still some issues that need to be solved. For example, how to increase the transmission distance of the quantum steer-

ing swapping remains a challenge. It is important and worthwhile to extend the quantum steering swapping to multipartite entangled states since rich and diverse steerabilities can be obtained after the quantum steering swapping.[57] It is also worthwhile to investigate applications of the steerabilities after quantum steering swapping and the extension of the protocol to DV and/or hybrid CV-DV systems.

In summary, we experimentally demonstrate the quantum steering swapping (quantum teleportation of quantum steering) between a CV GHZ state and a CV EPR state in a lossy channel. By choosing the gain in classical channels to optimize the steerabilities $\mathcal{G}^{A_1 \to A_2 B'_2}$ and $\mathcal{G}^{A_2 \to A_1 B'_2}$ the maximum transmission distance is achieved. The steerability between any two modes does not exist because of the monogamy relation. Only one-way and two-way steering of the collective steerabilities between one and the other two modes are presented in different ranges of transmission efficiency. The obtained collective quantum steerability from two to one modes $\mathcal{G}^{ij \to k}$ has potential application in QSS. Our results demonstrate the feasibility of establishing steerability between space-separated quantum nodes without direct interaction and make a step toward the application of quantum steering in quantum communication.

Supporting Information

Supporting Information is available from the Wiley Online Library or from the author.

Conflict of Interest

The authors declare no conflict of interest.

Data Availability Statement

The data that support the findings of this study are available from the corresponding author upon reasonable request.

Keywords

[1] M. Żukowski, A. Zeilinger, M. A. Horne, A. K. Ekert, *Phys. Rev. Lett.* **1993**, *71*, 4287.
[2] S. M. Tan, *Phys. Rev. A* **1999**, *60*, 2752.
[3] P. van Loock, S. L. Braunstein, *Phys. Rev. A* **1999**, *61*, 010302(R).
[4] V. N. Gorbachev, A. I. Zhiliba, A. I. Trubilko, *J. Opt. B: Quantum Semiclass. Opt.* **2001**, *3*, S25.
[5] J.-W. Pan, D. Bouwmeester, H. Weinfurter, A. Zeilinger, *Phys. Rev. Lett.* **1998**, *80*, 3891.
[6] C.-Y. Lu, T. Yang, J.-W. Pan, *Phys. Rev. Lett.* **2009**, *103*, 020501.
[7] X. Jia, X. Su, Q. Pan, J. Gao, C. Xie, K. Peng, *Phys. Rev. Lett.* **2004**, *93*, 250503.
[8] N. Takei, H. Yonezawa, T. Aoki, A. Furusawa, *Phys. Rev. Lett.* **2005**, *94*, 220502.
[9] X. Su, C. Tian, X. Deng, Q. Li, C. Xie, K. Peng, *Phys. Rev. Lett.* **2016**, *117*, 240503.
[10] S. Takeda, M. Fuwa, P. van Loock, A. Furusawa, *Phys. Rev. Lett.* **2015**, *114*, 100501.
[11] G. Guccione, T. Darras, H. Le Jeannic, V. B. Verma, S. Woo Nam, A. Cavaillés, J. Laurat, *Sci. Adv.* **2020**, *6*, eaba4508.
[12] S. Liu, Y. Lou, Y. Chen, J. Jing, *Phys. Rev. Lett.* **2022**, *128*, 060503.
[13] H. J. Kimble, *Nature* **2008**, *453*, 1023.
[14] S. Wehner, D. Elkous, R. Hanson, *Science* **2018**, *362*, eaam9288.
[15] A. Tavakoli, A. Pozas-Kerstjens, M.-X. Luo, M.-O. Renou, *Rep. Prog. Phys.* **2022**, *85*, 056001.
[16] A. Pozas-Kerstjens, N. Gisin, A. Tavakoli, *Phys. Rev. Lett.* **2022**, *128*, 010403.
[17] D. Cavalcanti, P. Skrzypczyk, *Rep. Prog. Phys.* **2017**, *80*, 024001.
[18] R. Uola, A. C. S. Costa, H. C. Nguyen, O. Gühne, *Rev. Mod. Phys.* **2020**, *92*, 015001.
[19] M. D. Reid, P. D. Drummond, W. P. Bowen, E. G. Cavalcanti, P. K. Lam, H. A. Bachor, U. L. Andersen, G. Leuchs, *Rev. Mod. Phys.* **2009**, *81*, 1727.
[20] Y. Xiang, S. Cheng, Q. Gong, Z. Ficek, Q. He, *PRX Quantum* **2022**, *3*, 030102.
[21] S. J. Jones, H. M. Wiseman, A. C. Doherty, *Phys. Rev. A* **2007**, *76*, 052116.
[22] H. M. Wiseman, S. J. Jones, A. C. Doherty, *Phys. Rev. Lett.* **2007**, *98*, 140402.
[23] E. G. Cavalcanti, S. J. Jones, H. M. Wiseman, M. D. Reid, *Phys. Rev. A* **2009**, *80*, 032112.
[24] A. Rutkowski, A. Buraczewski, P. Horodecki, M. Stobińska, *Phys. Rev. Lett.* **2017**, *118*, 020402.
[25] V. Händchen, T. Eberle, S. Steinlechner, A. Samblowski, T. Franz, R. F. Werner, R. Schnabel, *Nat. Photonics* **2012**, *6*, 596.
[26] C. Branciard, E. G. Cavalcanti, S. P. Walborn, V. Scarani, H. M. Wiseman, *Phys. Rev. A* **2012**, *85*, 010301(R).
[27] T. Gehring, V. Händchen, J. Duhme, F. Furrer, T. Franz, C. Pacher, R. F. Werner, R. Schnabel, *Nat. Commun.* **2015**, *6*, 8795.
[28] N. Walk, S. Hosseini, J. Geng, O. Thearle, J. Y. Haw, S. Armstrong, S. M. Assad, J. Janousek, T. C. Ralph, T. Symul, H. M. Wiseman, P. K. Lam, *Optica* **2016**, *3*, 634.
[29] M. Piani, J. Watrous, *Phys. Rev. Lett.* **2015**, *114*, 060404.
[30] S.-L. Chen, C. Budroni, Y.-C. Liang, Y.-N. Chen, *Phys. Rev. Lett.* **2016**, *116*, 240401.
[31] Q. He, L. Rosales-Zárate, G. Adesso, M. D. Reid, *Phys. Rev. Lett.* **2015**, *115*, 180502.
[32] C.-Y. Chiu, N. Lambert, T.-L. Liao, F. Nori, C.-M. Li, *npj Quantum Inf.* **2016**, *2*, 16020.
[33] Y. Xiang, I. Kogias, G. Adesso, Q. He, *Phys. Rev. A* **2017**, *95*, 010101(R).
[34] S. Armstrong, M. Wang, R. Y. Teh, Q. Gong, Q. He, J. Janousek, H. A. Bachor, M. D. Reid, P. K. Lam, *Nat. Phys.* **2015**, *11*, 167.
[35] D. Cavalcanti, P. Skrzypczyk, G. H. Aguilar, R. V. Nery, P. H. Souto Ribeiro, S. P. Walborn, *Nat. Commun.* **2015**, *6*, 7941.
[36] S. Wollmann, N. Walk, A. J. Bennet, H. M. Wiseman, G. J. Pryde, *Phys. Rev. Lett.* **2016**, *116*, 160403.
[37] K. Sun, X.-J. Ye, J.-S. Xu, X.-Y. Xu, J.-S. Tang, Y.-C. Wu, J.-L. Chen, C.-F. Li, G.-C. Guo, *Phys. Rev. Lett.* **2016**, *116*, 160404.
[38] Y. Xiao, X.-J. Ye, K. Sun, J.-S. Xu, C.-F. Li, G.-C. Guo, *Phys. Rev. Lett.* **2017**, *118*, 140404.
[39] X. Deng, Y. Xiang, C. Tian, G. Adesso, Q. He, Q. Gong, X. Su, C. Xie, K. Peng, *Phys. Rev. Lett.* **2017**, *118*, 230501.
[40] Z. Qin, X. Deng, C. Tian, M. Wang, X. Su, C. Xie, K. Peng, *Phys. Rev. A* **2017**, *95*, 052114.
[41] A. Cavaillès, H. Le Jeannic, J. Raskop, G. Guccione, D. Markham, E. Diamanti, M. D. Shaw, V. B. Verma, S. W. Nam, J. Laurat, *Phys. Rev. Lett.* **2018**, *121*, 170403.
[42] Y. Cai, Y. Xiang, Y. Liu, Q. He, N. Treps, *Phys. Rev. Res.* **2020**, *2*, 032046(R).
[43] M. Wang, Y. Xiang, H. Kang, D. Han, Y. Liu, Q. He, Q. Gong, X. Su, K. Peng, *Phys. Rev. Lett.* **2020**, *125*, 260506.
[44] L. Zeng, R. Ma, H. Wen, M. Wang, J. Liu, Z. Qin, X. Su, *Photonics Res.* **2022**, *10*, 777.
[45] S. Liu, D. Han, N. Wang, Y. Xiang, F. Sun, M. Wang, Z. Qin, Q. Gong, X. Su, Q. He, *Phys. Rev. Lett.* **2022**, *128*, 200401.
[46] Z.-Y. Hao, K. Sun, Y. Wang, Z.-H. Liu, M. Yang, J.-S. Xu, C.-F. Li, G.-C. Guo, *Phys. Rev. Lett.* **2022**, *128*, 120402.
[47] M. Fadel, T. Zibold, B. Décamps, P. Treutlein, *Science* **2018**, *360*, 409.
[48] P. Kunkel, M. Prüfer, H. Strobel, D. Linnemann, A. Frölian, T. Gasenzer, M. Gärttner, M. K. Oberthaler, *Science* **2018**, *360*, 413.
[49] C.-M. Li, K. Chen, Y.-N. Chen, Q. Zhang, Y.-A. Chen, J.-W. Pan, *Phys. Rev. Lett.* **2015**, *115*, 010402.
[50] C.-M. Li, H.-P. Lo, L.-Y. Chen, A. Yabushita, *Opt. Commun.* **2018**, *410*, 956.
[51] Q. Zeng, B. Wang, P. Li, X. Zhang, *Phys. Rev. Lett.* **2018**, *120*, 030401.
[52] Y. Guo, S. Cheng, X. Hu, B.-H. Liu, E.-M. Huang, Y.-F. Huang, C.-F. Li, G.-C. Guo, E. G. Cavalcanti, *Phys. Rev. Lett.* **2019**, *123*, 170402.
[53] R. V. Nery, M. M. Taddei, P. Sahium, S. P. Walborn, L. Aolita, G. H. Aguilar, *Phys. Rev. Lett.* **2020**, *124*, 120402.
[54] Y. Liu, K. Zheng, H. Kang, D. Han, M. Wang, L. Zhang, X. Su, K. Peng, *npj Quantum Inf.* **2022**, *8*, 38.
[55] X. Deng, Y. Liu, M. Wang, X. Su, K. Peng, *npj Quantum Inf.* **2021**, *7*, 65.
[56] M. Wang, Z. Qin, X. Su, *Phys. Rev. A* **2017**, *95*, 052311.
[57] M. Wang, Z. Qin, Y. Wang, X. Su, *Phys. Rev. A* **2017**, *96*, 022307.
[58] C. Weedbrook, S. Pirandola, R. García-Patrón, N. J. Cerf, T. C. Ralph, J. H. Shapiro, S. Lloyd, *Rev. Mod. Phys.* **2012**, *84*, 621.
[59] I. Kogias, A. R. Lee, S. Ragy, G. Adesso, *Phys. Rev. Lett.* **2015**, *114*, 060403.
[60] X. Su, A. Tan, X. Jia, J. Zhang, C. Xie, K. Peng, *Phys. Rev. Lett.* **2007**, *98*, 070502.
[61] M. D. Reid, *Phys. Rev. A* **2013**, *88*, 062108.
[62] X. Deng, C. Tian, M. Wang, Z. Qin, X. Su, *Opt. Commun.* **2018**, *421*, 14.